Supplementary Information for
A spatial-frequency patching metasurface enabling super-capacity perfect vector vortex beams

Zhipeng Yu[1,2,3,†], Xinyue Gao[1,†], Jing Yao[2,3], Zhiyuan Wang[2,3], Tianting Zhong[2,3], Yuzhi Shi[4], Bo Li[1,5], Puxiang Lai[2,3,6,*], Xiangping Li[7,*], and Qinghua Song[1,5,*]

[1]Tsinghua Shenzhen International Graduate School, Tsinghua University, Shenzhen, Guangdong, China

[2]Department of Biomedical Engineering, Hong Kong Polytechnic University, Hong Kong SAR, China

[3]Hong Kong Polytechnic University Shenzhen Research Institute, Shenzhen, Guangdong, China

[4]Institute of Precision Optical Engineering, School of Physics Science and Engineering, Tongji University, Shanghai 200092, China

[5]Suzhou Laboratory, Suzhou 215000, China

[6]Photonics Research Institute, Hong Kong Polytechnic University, Hong Kong SAR, China

[7]Guangdong Provincial Key Laboratory of Optical Fiber Sensing and Communications, Institute of Photonics Technology, Jinan University, Guangzhou 510632, China

[†]These authors contributed equally to this work.

*Corresponding email: puxiang.lai@polyu.edu.hk; xiangpingli@jnu.edu.cn; song.qinghua@sz.tsinghua.edu.cn

Supplementary Note S1: Demonstration of patching arbitrary partial elliptical arcs.

Here we provide a general method to patch unlimited number of elliptic seamless arcs, as illustrated in Supplementary Fig. S1. To demonstrate the concept, we focus on patching two partial elliptic arcs. As depicted in Supplementary Fig. S1a, the procedure of patching a partial elliptic arc with a partial circular arc is divided into four distinct steps:

(I) A red dashed line intersects an ellipse at a single point, indicated by a black cross, while the blue dashed line represents the tangent to the ellipse at this point. The ellipse intersects the upper half of the vertical axis at another point, also marked by a black cross. The partial segment between these two crosses is the area designated for tailoring.

(II) The blue dashed tangent line from Step I is parallelly transferred to touch a circle at a single point, denoted by a cross. A green line extending from the origin through the tangency point is introduced. An arbitrary point on the circle is selected and marked with a cross. Similarly, the partial arc is tailored between these two crosses.

(III) The two segments from Steps I and II are maintained in their original positions for the patching process in the following step.

(IV) While the elliptical arc remains fixed, the circular arc is relocated either perpendicularly or parallel to the tangent line to merge with the elliptical arc at the tangency point.

Removing all auxiliary lines, a smooth patched partial segment is obtained, as shown in the final column of Supplementary Fig. S1a. A similar technique can be applied for patching two elliptical arcs, as demonstrated in Supplementary Fig. S1b. By repeatedly applying this method to patch different partial arcs, a SC-PVB that incorporates any number of arbitrary partial arcs with a seamless and smooth ring can be generated. Therefore, the maximum number of arcs should theoretically be infinite.

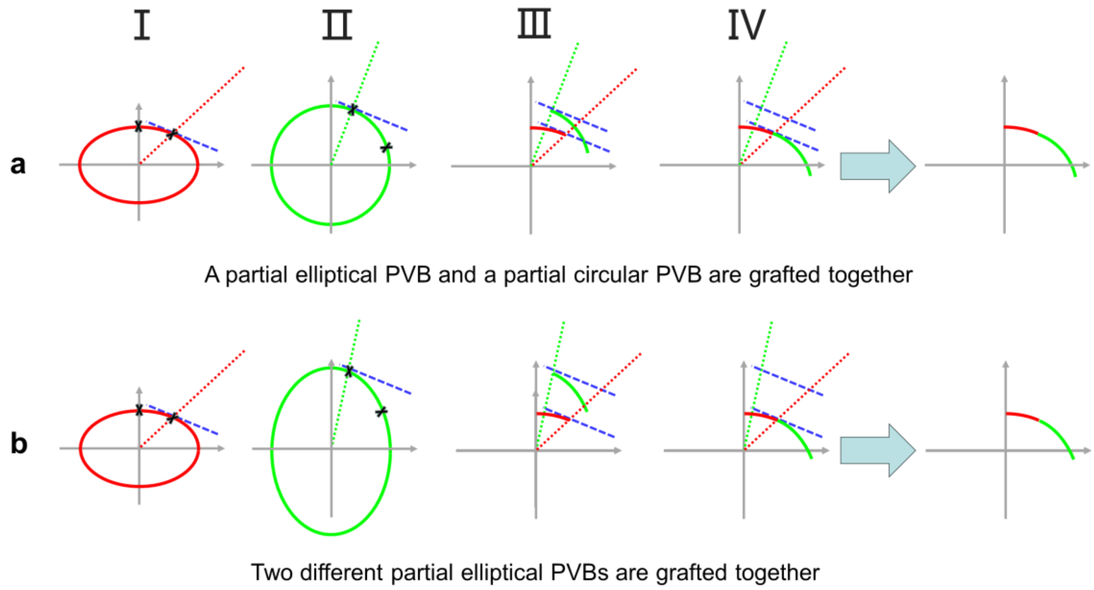

Figure S1. Principle of patching arbitrary partial elliptical PVBs. (a) Patching a partial elliptical arc with a partial circular arc. (b) Patching two partial elliptical arcs with different sizes.

Supplementary Note S2: Some criteria for normalizing factors and TCs to obtain a seamless and smooth ring.

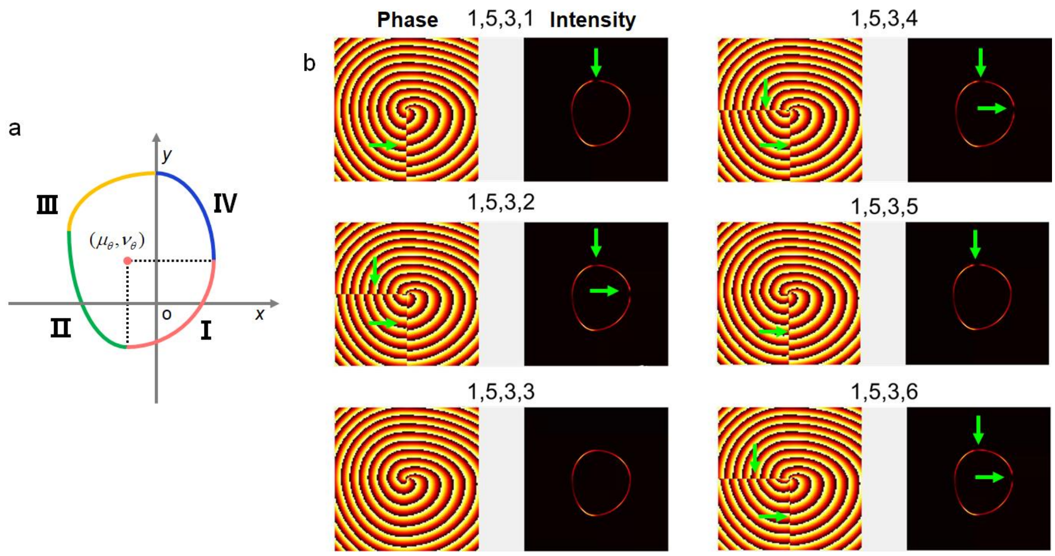

Figure S2. Discontinuity analysis of the SC-PVB. (a) Two schematic diagrams are used to describe horizontal (vertical) normalizing factors relationship among four segments. (b) Phase profile and intensity profiles of different combinations of TCs for segments of a SC-PVB. Green arrows indicate observable abrupt changes in the phase profile and the appearance of singularities—such as a breaking point or a sudden decrease in size.

In order to achieve a seamless and smooth ring without discontinuity, the horizontal and vertical normalizing factors of the four segments a_i and b_i must adhere to the following relationship:

$$1/a_1 + 1/a_2 = 1/a_3 + 1/a_4 \tag{S1}$$

$$1/b_1 + 1/b_4 = 1/b_2 + 1/b_3 \tag{S2}$$

Tangent lines of all segments at all intersections are parallel to the horizontal or vertical axis, which is the prerequisite of forming a smooth ring. The length of each segment along the horizontal axis is linearly related to the reciprocal of its corresponding horizontal normalizing factor. To achieve a seamless patching of these four segments as depicted in Supplementary Fig. S2a, the lengths of the upper and lower semi-rings along the horizontal and vertical axes must be equivalent. This requirement is in accordance with the principles outlined in Eqs. S1 and S2.

The equivalent TC (ETC) of SC-PVB could be given by $l_{SC}=\frac{l_1+l_2+l_3+l_4}{4}$. If l_{SC} is an integer, the TC of the SC-PVB splits into l_{GE} unit TCs which is similar to that of the PVB. The TC difference between each group of two adjacent segments should be taken into consideration. To make l_{SC} an integer and the ring without breakpoints, the necessary condition is that the TC difference of arbitrary two adjacent segments is an integer multiple of 4:

$$l_1-l_2=4g;l_3-l_4=4h;l_2-l_3=4k;(g,h,k\in\mathbb{Z}) \tag{S3}$$

In our work, segments I and II (segments III and IV) compose upper (lower) half. Each half part constructs a semi-ring, in which each part can be regarded as a half vortex and TCs of upper and lower half vortex are $\frac{l_1+l_2}{2}$ and $\frac{l_3+l_4}{2}$. To make l_{GE} an integer, the sufficient and necessary condition is that the difference between $\frac{l_1+l_2}{2}$ and $\frac{l_3+l_4}{2}$ should be an integer multiple of 2. At the same time, the TC relationship between segments II and III (as well as segments I and IV) constrained in Eq. S3 can be weaken. As a result, the TC relationship among these four segments can be furtherly constrained by:

$$\begin{gathered}l_1-l_2=4g;l_3-l_4=4h(g,h,k\in\mathbb{Z})\\ \frac{l_1+l_2}{2}-\frac{l_3+l_4}{2}=2f(f\in\mathbb{Z})\end{gathered} \tag{S4}$$

The TC relationship among all segments can be furtherly simplified by organizing and simplifying Eq. S4:

$$l_1-l_2=4g;l_3-l_4=4h;l_1-l_3=2k;(g,h,k\in\mathbb{Z}) \tag{S5}$$

When the ETC is a non-integer especially a half integer, one of the singularities of the SC-PVB is located at the horizontal axis of the annular gap. This phenomenon is the same as the fractional OV. The reason is that a fractional phase jump occurs at the object plane when the ETC is not an integer. Supplementary Fig. S2c show different simulated results with TCs not conforming to Eq. S5. In a SC-PVB, with fixed TCs of 1, 5, and 3 set in Segments I, II, and III, respectively, altering the TC in Segment IV from 1 to 6 results in observable abrupt changes in the phase profile and the appearance of singularities, such as a breaking point or a sudden decrease, in the intensity profile with various TCs. Notably, when the TC is set to 3, the effective transmission coefficient (ETC) becomes an integer, and under this condition, the SC-PVB does not exhibit any singularities.

Supplementary Note S3: Summary of experiment results and associated parameters in Figs. 4c and 4d in the main text

Table S1 Summary of experiment results in Fig. 4c of the main text.

Shape	I: 0.78; II: 1.03 III: 1.45;
Polarization order	I: 2; II: 1 III: 2
Ellipticity angle	I: 0°; II: ~-22° III: ~23°;

Table S2 Summary of experiment results in Fig. 4d of the main text.

Shape	I: 0.79; II: 1.23
Polarization order	I: 3; II: 2
Ellipticity angle	I: 0°; II: ~-20°

Supplementary Note S4: Broadband generation of SC-PVVB using a geometric metasurface

Supplementary Fig. S3 presents the experimental outcomes for the SC-PVVB at the wavelengths of 460 nm, 532 nm, and 650 nm. The intensity profiles at these wavelengths, as shown in Supplementary Fig. S3a, are nearly identical, with magnification increasing from 460 nm to 650 nm due to the optical diffraction effects of the grating. Supplementary Figs. S3b and S3c show the polarization azimuth and ellipticity angles of the SC-PVVB at these wavelengths, respectively, as quantified by Stokes parameter measurements. These results indicate a high degree of consistency across the wavelengths. The near-identical measurements of the polarization azimuth and ellipticity angles across the three wavelengths, as shown in Supplementary Figs. S3b and S3c, demonstrate the metasurface platform's ability to reliably generate beams with the desired polarization states across a broad spectral range, facilitated by the geometric metasurface design.

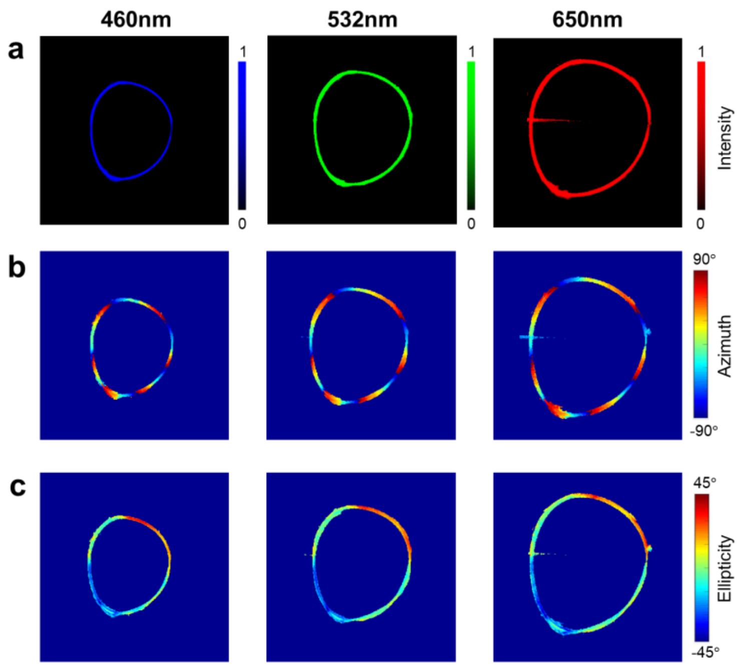

Figure S3. Verification of broadband generation of SC-PVVB using a geometric metasurface due to the broadband characteristic of the geometric phase. (a) Intensity profiles, (b) azimuth angle and (c) ellipticity angle of polarization of the SC-PVVB at different wavelengths.

Supplementary Note S5: Simulated and experimental results of SC-PVVB propagating in free space.

To demonstrate the propagation characteristics of the SC-PVVB in free space, both simulated and experimental results are presented. The simulated images, which illustrate the SC-PVVB's propagation in free space, are shown in Supplementary Fig. S4. It is observed that the shape of the SC-PVVB remains consistent beyond a propagation distance of 10 mm. Furthermore, the experimental results, detailed in Supplementary Fig. S5, corroborate these findings. In the experimental setup, an aspheric lens (f = 16 mm) with a numerical aperture (NA) of 0.65 is placed behind the metasurface to perform a Fourier transform on the optical field in the metasurface plane, following the configuration described in the main text. A camera is first positioned in the Fourier plane (z = 0) to capture the optical field. Subsequently, the camera is moved to positions at 10 mm, 20 mm, and 30 mm to record the optical field at these distances. The experimental data reveal that the shape and intensity distribution of the optical field are essentially maintained across these varying distances.

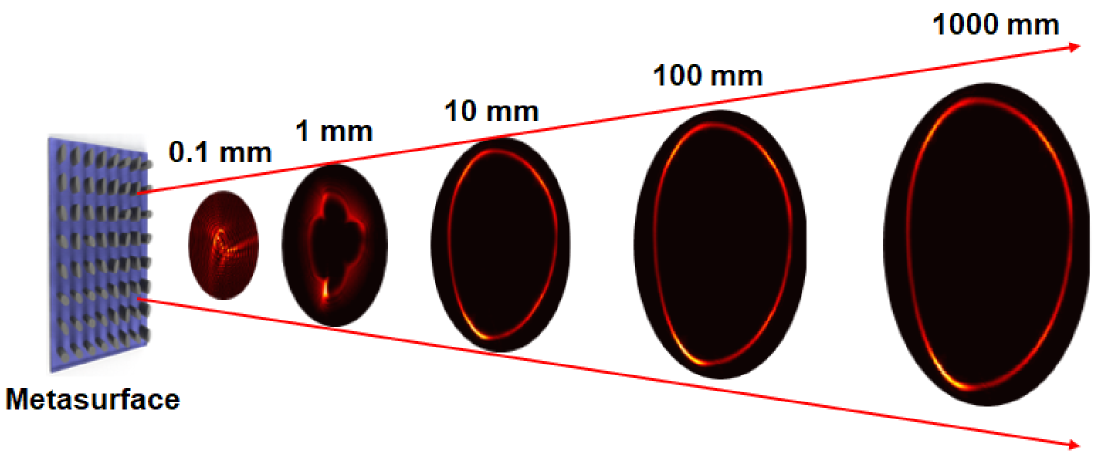

Figure S4. The simulated propagation characteristics of the SC-PVVB in free space.

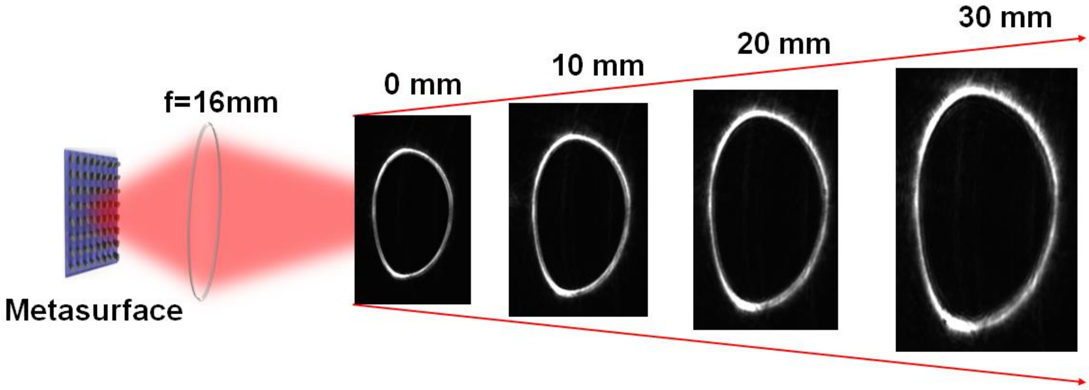

Figure S5. The experimental propagation characteristics of the SC-PVVB in free space.

Supplementary Note S6: An optimized Dammann grating capable of supporting a distinct SC-PVVB in every diffraction order.

A random phase function has been proven to reduce crosstalk among different holograms(*1*). Here similar procedure can be introduced to optimize the Dammann grating, facilitating the accurate modulation of the optical field across all orders. As depicted in Supplementary Figs. S6g-h, it is possible to concentrate the optical power in specific orders by introducing a random phase profile. However, this method often results in significant fluctuations in power across the various orders. To address this issue, we employ a genetic algorithm to optimize the phase profile, aiming to minimize power fluctuations and enhance the performance of the grating. The loss function used for this optimization is defined as follows:

$$Loss = \frac{std(\{I_k\})}{mean(\{I_k\})}, k = 1,2,3...K \tag{S6}$$

where K is the number of all target diffraction orders. $\{I_k\}$represents the set of intensities of all target diffraction orders. As demonstrated in Supplementary Figs. S6a and S6d, we achieve a uniform distribution of optical power concentrated within a 4*4 array of these orders. Quantitatively, the resulting loss value in Eq. S6 is 0.0057, with 93.57% of the total power successfully directed into the target orders. The optimized phase profile, denoted as (ρ), which contributes to this result, is depicted in the top right corner of Supplementary Fig. S6d. Utilizing the same optimized phase profile, we further customize the optical field for each target order. Specifically, the intensities in the first and third columns of orders are designed to be uniform and twice the intensity of the other orders. The simulation results, as presented in Supplementary Figs. S6b and S3e, closely align with our desired outcomes. This methodology can be extended to accommodate a greater number of diffraction orders, as evidenced by the results in Supplementary Figs. S6c and S6f, which pertain to a 6*6 array of orders.

The required phase profile of carrying a distinct SC-PVVB in each order of Dammann grating with the optimized phase can be expressed by:

$$\phi = \arg\left\{\sum_{m=-\infty}^{0}\sum_{n=-\infty}^{+\infty}\left[E_R(m,n)e^{i(\phi_{SC-PVB\_R(m,n)}+\frac{2m\pi}{T}x+\frac{2n\pi}{T}y+\rho(m,n))}+E_L(m,n)e^{i(-\phi_{SC-PVB\_L(m,n)}-\frac{2m\pi}{T}x-\frac{2n\pi}{T}y+\rho(-m,-n))}\right]\right\} \quad (S7)$$

where m and n are the indexes of the corresponding order. T is the period of the grating. As shown in Supplementary Fig. S7, the intensity and polarization azimuth angle distributions are centrosymmetric and the polarization ellipticity angle distribution is skew-centrosymmetric, which agree well with the design. Since the left and right halves of the optical field contain the same information, only the left half is used for information transmission in the main text.

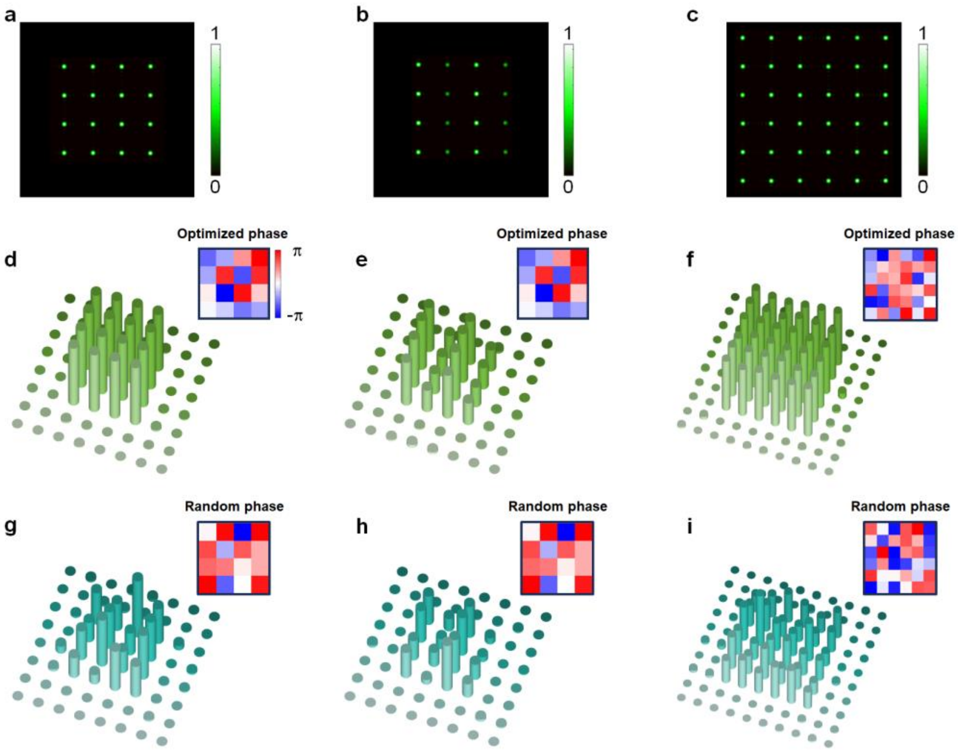

Figure S6. The simulated result of a Dammann grating with optimized a phase profile and a random phase profile. (a-f) images and statistical histograms of intensity distribution with an optimized phase profile for the customized light intensity distribution in corresponding diffraction orders. (g-i) statistical histograms of intensity distribution with a random phase profile for the customized light intensity distribution in corresponding diffraction orders.

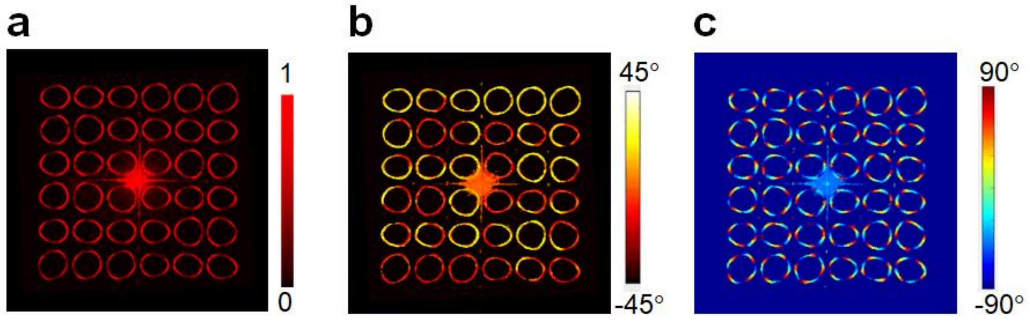

Figure S7. Experiment results of whole optical field in Fig.5 in the main text. (a) Intensity profile, (b) ellipticity angle and (c) azimuth angle of polarization of the 6*6 array of distinct SC-PVVB.

Supplementary Note S7: Simulated results of SC-PVVB array propagating in free space.

To demonstrate the propagation characteristics of the SC-PVVB array in free space, simulated results are presented. The simulated images, which illustrate the SC-PVVB array's propagation in free space, are shown in Supplementary Fig. S8. It is observed that the shape of the SC-PVVB array also remains consistent beyond a propagation distance of 10 mm.

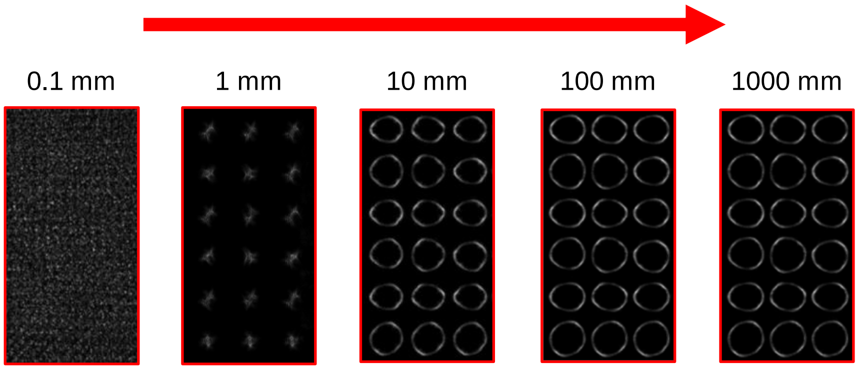

Figure S8. The simulated propagation characteristics of the SC-PVVB array in free space.

REFERENCES

1. H. Ren, X. Fang, J. Jang, J. Bürger, J. Rho, S. A. Maier, Complex-amplitude metasurface-based orbital angular momentum holography in momentum space. *Nat. Nanotechnol.* **15**, 948-955 (2020).